Refined 1D finite elements for the analysis of secondary, primary and complete civil engineering structure

REFINED 1D FINITE ELEMENTS FOR THE ANALYSIS OF SECONDARY, PRIMARY AND COMPLETE CIVIL ENGINEERING STRUCTURE

Erasmo Carrera [1], Alfonso Pagani [2], and Marco Petrolo [3]

ABSTRACT

This paper proposes the use of an advanced one-dimensional (1D) variable kinematic model to analyze typical civil engineering structures. The model is referred to as Component-Wise (CW) and it was originally introduced for the analysis of multilayered plate and shell structures. The CW approach is based on the Carrera Unified Formulation (CUF). CUF can be used for the straightforward development of a large variety of classical and refined beam theories which are able to capture three-dimensional stress/strain states and non-classical phenomena such as the in-plane warping of the cross-section. CUF can be seen as a hierarchical formulation since it has variable kinematic features; 1D models with arbitrarily chosen accuracy can be obtained, including the classical Euler-Bernoulli and Timoshenko beam theories. CUF models are formulated in terms of fundamental nuclei whose expressions are formally independent of the adopted hierarchical scheme. Lagrange polynomials are used in the proposed CW models to expand the displacement field of the beam above the cross-section. The finite element method was used in this work to obtain numerical solutions. The conducted numerical investigation shows that CW models can be successfully applied to

[1]Professor. Deptartment of Mechanical and Aerospace Engineering, Politecnico di Torino, Corso Duca degli Abruzzi 24, 10129 Torino, Italy. AND School of Aerospace, Mechanical and Manufacturing Engineering RMIT University, Bundoora VIC 3083, Australia. *E-mail address:* erasmo.carrera@polito.it

[2]Ph.D. Student. Deptartment of Mechanical and Aerospace Engineering, Politecnico di Torino, Corso Duca degli Abruzzi 24, 10129 Torino, Italy. *E-mail address:* alfonso.pagani@polito.it

[3]Research Fellow. School of Aerospace, Mechanical and Manufacturing Engineering RMIT University, Bundoora VIC 3083, Australia. *E-mail address:* marco.petrolo@rmit.edu.au

any geometries with no restrictions on the ratio between the cross-sectional dimensions and the length of the beam. A very short C-shaped beam was therefore used to analyze a classical portal frame. Similarly, analyses of truss-structures and a full industrial-construction were carried out. Classical beam/plate/solid finite elements as well as combinations of them were used to obtain solutions from the commercial code MSC Nastran for comparison purposes. The results show the effectiveness of the CW approach both in terms of accuracy and computational efficiency.

Keywords: Refined Beam Theories, Finite Elements, Carrera Unified Formulation, Civil Structures, Component-Wise.

INTRODUCTION TO REFINED 1D THEORIES

Beam models are widely used to analyze the mechanical behavior of slender bodies, such as columns, rotor-blades, aircraft wings, towers, antennae and bridges, amongst others. The simplicity of one-dimensional (1D) theories and their ease of application coupled with their computational efficiency are some of the main reasons why structural analysts prefer beams to two-dimensional (2D) and three-dimensional (3D) models.

The classical and best-known beam theories are those by Euler 1744 (hereinafter referred to as EBBM) and Timoshenko (Timoshenko 1922a; Timoshenko 1922b) (hereinafter referred to as TBM). The former does not account for transverse shear deformations and rotatory inertia, whereas the latter assumes a uniform shear distribution along the cross-section of the beam together with the effects of rotatory inertia.

If the rectangular cartesian coordinate system shown in Fig. 1 is adopted and we consider bending on the xy-plane, the kinematic field of EBBM can be written as follows:

$$\begin{aligned} u &= u^0 \\ v &= v^0 - x\,\frac{\partial u^0}{\partial y} \end{aligned} \tag{1}$$

where u and v are the displacement components of a point belonging to the beam domain along x and y coordinates, respectively. u^0 and v^0 are the displacements of the beam axis,

whereas $-\dfrac{\partial u^0}{\partial y}$ is the rotation of the cross-section about the z-axis (i.e. ϕ_z) as shown in Fig. 2a. According to EBBM, the deformed cross-section remains plane and orthogonal to the beam axis.

EBBM neglects the cross-sectional shear deformation phenomena. Generally, the shear stresses play an important role in several problems (e.g. short beams, composite structures) and neglecting these terms can lead to incorrect results. One may want to generalize Eq. (1) and overcome the EBBM assumption of the orthogonality of the cross-section. The improved displacement field results in the TBM,

$$\begin{aligned} u &= u^0 \\ v &= v^0 + x\ \phi_z \end{aligned} \tag{2}$$

TBM constitutes an improvement over EBBM since the cross-section does not necessarily remain perpendicular to the beam axis after deformation and one degree of freedom (i.e. the unknown rotation ϕ_z) is added to the original displacement field (see Fig. 2b).

Classical beam models yield reasonably good results when slender, solid section, homogeneous structures are subjected to bending. Conversely, the analysis of deep, thin-walled, open section beams may require more sophisticated theories to achieve sufficiently accurate results, see (Novozhilov 1961). One of the main problems of TBM is the homogeneous conditions of the transverse stress components at the top/bottom surfaces of the beam are not fulfilled, as shown in Fig. 3. One can impose, for instance, Eq. (2) in order to have null transverse strain component ($\gamma_{xy} = \frac{\partial u}{\partial y} + \frac{\partial v}{\partial x}$) at $x = \pm\frac{b}{2}$. This leads to the third-order displacement field known as the Valsov beam theory (Vlasov 1961)

$$\begin{aligned} u &= u^0 \\ v &= v^0 + f_1(x)\ \phi_z + g_1(x)\ \frac{\partial u^0}{\partial y} \end{aligned} \tag{3}$$

where $f_1(x)$ and $g_1(x)$ are cubic functions of the x coordinate. It should be noted that al-

though the model of Eq. (3) has the same number of degrees of freedom (DOFs) of TBM, it overcomes classical beam theory limitations by foreseeing a quadratic distribution of transverse stresses on the cross-section of the beam.

The above theories are not able to include any kinematics resulting from the application of torsional moments. The simplest way to include torsion consists at considering a rigid rotation of the cross-section around the y-axis (i.e. ϕ_y), see Fig. 4. The resulting displacement model is:

$$\begin{aligned} u &= z\ \phi_y \\ w &= -x\ \phi_y \end{aligned} \tag{4}$$

where w is the displacement component along the z-axis. According to Eq. (4), a linear distribution of transverse displacement components is needed to detect the rigid rotation of the cross-section about the beam axis.

Beam models which include all the capabilities discussed so far can be obtained by summing all these contributions. By considering the deformations also in the yz-plane, one has

$$\begin{aligned} u &= u^0 + z\ \phi_y \\ v &= v^0 + f_1(x)\ \phi_z + f_2(z)\ \phi_x + g_1(x)\ \frac{\partial u}{\partial y} + g_2(z)\ \frac{\partial w}{\partial y} \\ w &= w^0 - x\ \phi_y \end{aligned} \tag{5}$$

where $f_1(x)$, $g_1(x)$, $f_2(z)$, and $g_2(z)$ are cubic functions *. The beam models discussed so far are not able to account for many *higher-order effects*, such as the second-order in-plane deformations of the cross-section.

Over the last century, many refined beam theories have been proposed to overcome the limitations of classical beam modelling. A commendable and comprehensive review on beam theories con be found in (Kapania and Raciti 1989a; Kapania and Raciti 1989b). Different

*In the case of rectangular cross-section, the cubic functions from Vlasov's theory are

$$f_1(x) = x - \frac{4}{3b^2}x^3, \qquad g_1(x) = -\frac{4}{3b^2}x^3, \qquad f_2(z) = z - \frac{4}{3h^2}z^3, \qquad g_2(z) = -\frac{4}{3h^2}z^3$$

where b and h are the dimensions of the cross-section along the x- and z-axis, respectively.

approaches have been used to improve the beam models, which include the use of warping functions based on de Saint-Venant's solution (El Fatmi 2002; El Fatmi 2007a; El Fatmi 2007b; Ladéveze and Simmonds 1998; Ladéveze et al. 2004; Rand 1994; Kim and White 1997), the variational asymptotic solution (VABS) (Berdichevsky et al. 1992; Volovoi et al. 1999; Popescu and Hodges 2000; Yu et al. 2002; Yu and Hodges 2004; Yu and Hodges 2005; Kim and Wang 2010; Firouz-Abad et al. 2007), the generalized beam theory (GBT) (Schardt 1966; Schardt 1994; Silvestre and Camotim 2002; Silvestre 2002; Silvestre 2007; Bebiano et al. 2008). A displacement field which is able to take into account the cross-section deformation by means of warping functions is

$$\begin{aligned} u &= u^0 \\ v &= v^0 + \mathtt{f}(x)\ \epsilon^0_{xy} - x\ \frac{\partial u^0}{\partial y} + \mathtt{f}(z)\ \epsilon^0_{yz} - z\ \frac{\partial w^0}{\partial y} \\ w &= w^0 \end{aligned} \tag{6}$$

where $\mathtt{f}(x)$ and $\mathtt{f}(z)$ are the warping functions, whereas ϵ^0_{xy} and ϵ^0_{yz} are the transverse shear strains measured on the beam axis. As a general guideline, one can state that the richer the kinematic field, the more accurate the 1D model becomes (Washizu 1968). The main disadvantages of a reacher displacement field are: the increase of equations to be solved and the choice of the terms to be added since this choice is generally problem dependent.

The Carrera Unified Formulation (CUF) (Carrera et al. 2011a) represents a tool to tackle the problem of the choice of the expansion terms. Let $\mathbf{u} = \{u_x\, u_y\, u_z\}^T$ be the transposed displacement vector. According to CUF, the generic displacement field can be expressed in a compact manner as an N-order expansion in terms of generic functions, F_τ,

$$\mathbf{u}(x, y, z) = F_\tau(x, z)\mathbf{u}_\tau(y), \qquad \tau = 1, 2, ..., M \tag{7}$$

where F_τ are the functions of the coordinates x and z on the cross-section. $\mathbf{u}_\tau$ is the vector of the *generalized displacements*, M stands for the number of terms used in the expansion. In

line with Eq. (7), Eq.s (1) to (5) consist of MacLaurin expansions that uses 2D polynomials $x^i\, z^j$ as base functions, where i and j are positive integers. This class of models is referred to as TE (Taylor-Expansion). It should be noted that Eq.s (1), (2), and (4) are particular cases of the linear ($N = 1$) TE model, which can be expressed as

$$\begin{aligned} u_x &= u_{x_1} + x\ u_{x_2} + z\ u_{x_3} \\ u_y &= u_{y_1} + x\ u_{y_2} + z\ u_{y_3} \\ u_z &= u_{z_1} + x\ u_{z_2} + z\ u_{z_3} \end{aligned} \tag{8}$$

where the parameters on the right-hand side (u_{x_1}, u_{y_1}, u_{z_1}, u_{x_2}, etc.) are the displacements and the rotations of the beam reference axis. Higher-order terms can be took into account according to Eq.(7). For instance, the displacement fields of Eq.s (3) and (5) can be seen as particular cases of the third-order ($N = 3$) TE model

$$\begin{aligned} u_x &= u_{x_1} + x\ u_{x_2} + z\ u_{x_3} + x^2\ u_{x_4} + xz\ u_{x_5} + z^2\ u_{x_6} + x^3\ u_{x_7} + x^2z\ u_{x_8} + xz^2\ u_{x_9} + z^3\ u_{x_{10}} \\ u_y &= u_{y_1} + x\ u_{y_2} + z\ u_{y_3} + x^2\ u_{y_4} + xz\ u_{y_5} + z^2\ u_{y_6} + x^3\ u_{y_7} + x^2z\ u_{y_8} + xz^2\ u_{y_9} + z^3\ u_{y_{10}} \\ u_z &= u_{z_1} + x\ u_{z_2} + z\ u_{z_3} + x^2\ u_{z_4} + xz\ u_{z_5} + z^2\ u_{z_6} + x^3\ u_{z_7} + x^2z\ u_{z_8} + xz^2\ u_{z_9} + z^3\ u_{z_{10}} \end{aligned} \tag{9}$$

The possibility of dealing with any-order expansion makes the TE CUF able to handle arbitrary geometries, thin-walled structures and local effects as it has been shown for both static (Carrera et al. 2010; Carrera et al. 2012d) and free-vibration analyses (Carrera et al. 2011b; Carrera et al. 2012c; Petrolo et al. 2012).

Recently, a new class of CUF models has been developed by the first author and his co-workers (Carrera and Petrolo 2012a; Carrera et al. 2012b). In this class of models, Lagrange-like polynomials are used to discretize the displacement field on the cross-section. These models are referred to as Component-wise (CW). Static analyses on isotropic (Carrera and Petrolo 2012a) and composite structures (Carrera and Petrolo 2012b; Carrera et al. 2012a) have revealed the strength of CW models in dealing with open cross-sections, localized

boundary conditions and layer-wise descriptions of composite structures. Moreover, both static (Carrera et al. 2013a) and dynamic (Carrera et al. 2013b) analysis of reinforced-shell wing structures by 1D CW models have been carried out and the results have shown the enhanced capabilities of CW in obtaining 3D accuracy with very low computational costs.

In the present paper, CW models are extended to the static analysis of secondary, primary and complete civil constructions. In the next section CW models are formulated by using CUF. 1D refined elements are then obtained by classical finite element (FE) approximation. Numerical results are subsequently discussed. Finally, the main conclusions are outlined.

THE COMPONENT-WISE APPROACH VIA CUF

The degrees of freedom of the TE models (displacements and N-order derivatives of displacements) described above are defined along the axis of the beam. The unknown variables are only pure displacements if Lagrange polynomials are adopted as expansion functions (F_τ) in Eq. (7). The resulting approach is referred to as Component-wise since Lagrange elements are used to model the displacement variables in each structural component at the cross-sectional level.

In this work, three types of cross-sectional polynomial sets were adopted as shown in Fig. 5: three-point elements (L3), four-point elements (L4), and nine-point elements (L9). The isoparametric formulation was exploited to deal with arbitrary shaped geometries. The Lagrange polynomial expansions can be found in (Oñate 2009). The interpolation functions in the case of an L4 element are, for example,

$$F_\tau = \frac{1}{4}(1 + r\ r_\tau)(1 + s\ s_\tau) \qquad \tau = 1, 2, 3, 4 \tag{10}$$

where r and s vary from -1 to $+1$, whereas r_τ and s_τ are the coordinates of the four points whose numbering and location in the natural coordinate frame are shown in Fig. 5b. The

displacement field given by an L4 element is

$$\begin{aligned} u_x &= F_1\, u_{x_1} + F_2\, u_{x_2} + F_3\, u_{x_3} + F_4\, u_{x_4} \\ u_y &= F_1\, u_{y_1} + F_2\, u_{y_2} + F_3\, u_{y_3} + F_4\, u_{y_4} \\ u_z &= F_1\, u_{z_1} + F_2\, u_{z_2} + F_3\, u_{z_3} + F_4\, u_{z_4} \end{aligned} \tag{11}$$

where $u_{x_1}, ..., u_{z_4}$ are the displacement variables of the problem and represent the translational displacement components of each of the four points of the L4 element. For further refinements, the cross-section can be discretized by using several L-elements as in Fig. 6, where two assembled L9 elements are shown. This is one of the main feature of the CW approach.

Most of the engineering structures are composed by different components, such as columns and walls or flanges and webs in the case of typical civil constructions. However, these components usually have different geometries and scales. The CW models each typical component of a structure through the 1D CUF formulation. In a finite element framework, this means that different components are modelled by means of the same 1D finite element, i.e. the same stiffness matrix is used for each component.

The CW methodology allows us to tune the capabilities of the model by (1) choosing which component requires a more detailed model; (2) setting the order of the structural model to be used. Moreover, via the CW approach, FE mathematical models can be built by using only physical boundaries; artificial lines (beam axes) and surfaces (plate/shell reference surfaces) are no longer necessary.

FINITE ELEMENT FORMULATION

Preliminaries

Referring to the coordinate frame shown in Fig. 1, let the cross-section of the structure be denoted by Ω and the beam boundaries over y be $0 \leq y \leq L$. The stress, $\boldsymbol{\sigma}$, and strain,

$\boldsymbol{\epsilon}$, components are grouped as follows:

$$\begin{aligned} \boldsymbol{\sigma}_p &= \left\{ \begin{array}{ccc} \sigma_{zz} & \sigma_{xx} & \sigma_{zx} \end{array} \right\}^T, \quad \boldsymbol{\epsilon}_p = \left\{ \begin{array}{ccc} \epsilon_{zz} & \epsilon_{xx} & \epsilon_{zx} \end{array} \right\}^T \\ \boldsymbol{\sigma}_n &= \left\{ \begin{array}{ccc} \sigma_{zy} & \sigma_{xy} & \sigma_{yy} \end{array} \right\}^T, \quad \boldsymbol{\epsilon}_n = \left\{ \begin{array}{ccc} \epsilon_{zy} & \epsilon_{xy} & \epsilon_{yy} \end{array} \right\}^T \end{aligned} \tag{12}$$

The subscript "n" stands for terms lying on the cross-section, while "p" stands for terms lying on planes which are orthogonal to Ω. In the case of small displacements with respect to a characteristic dimension of Ω, linear strain - displacement relations can be used

$$\begin{aligned} \boldsymbol{\epsilon}_p &= \boldsymbol{D}_p \mathbf{u} \\ \boldsymbol{\epsilon}_n &= \boldsymbol{D}_n \mathbf{u} = (\boldsymbol{D}_{n\Omega} + \boldsymbol{D}_{ny}) \mathbf{u} \end{aligned} \tag{13}$$

where $\boldsymbol{D}_p$ and $\boldsymbol{D}_n$ are linear differential operators based on small displacement theory,

$$\boldsymbol{D}_p = \begin{bmatrix} 0 & 0 & \frac{\partial}{\partial z} \\ \frac{\partial}{\partial x} & 0 & 0 \\ \frac{\partial}{\partial z} & 0 & \frac{\partial}{\partial x} \end{bmatrix}, \quad \boldsymbol{D}_{n\Omega} = \begin{bmatrix} 0 & \frac{\partial}{\partial z} & 0 \\ 0 & \frac{\partial}{\partial x} & 0 \\ 0 & 0 & 0 \end{bmatrix}, \quad \boldsymbol{D}_{ny} = \begin{bmatrix} 0 & 0 & \frac{\partial}{\partial y} \\ \frac{\partial}{\partial y} & 0 & 0 \\ 0 & \frac{\partial}{\partial y} & 0 \end{bmatrix} \tag{14}$$

Linear elastic constitutive laws were exploited to obtain stress components,

$$\boldsymbol{\sigma} = \boldsymbol{C} \boldsymbol{\epsilon} \tag{15}$$

According to Eq.s (12), Eq. (15) becomes

$$\begin{aligned} \boldsymbol{\sigma}_p &= \tilde{\boldsymbol{C}}_{pp} \boldsymbol{\epsilon}_p + \tilde{\boldsymbol{C}}_{pn} \boldsymbol{\epsilon}_n \\ \boldsymbol{\sigma}_n &= \tilde{\boldsymbol{C}}_{np} \boldsymbol{\epsilon}_p + \tilde{\boldsymbol{C}}_{nn} \boldsymbol{\epsilon}_n \end{aligned} \tag{16}$$

In the case of isotropic material the matrices $\tilde{\boldsymbol{C}}_{pp}$, $\tilde{\boldsymbol{C}}_{nn}$, $\tilde{\boldsymbol{C}}_{pn}$, and $\tilde{\boldsymbol{C}}_{np}$ are

$$\tilde{\boldsymbol{C}}_{pp} = \begin{bmatrix} \lambda+2G & \lambda & 0 \\ \lambda & \lambda+2G & 0 \\ 0 & 0 & G \end{bmatrix}, \quad \tilde{\boldsymbol{C}}_{nn} = \begin{bmatrix} G & 0 & 0 \\ 0 & G & 0 \\ 0 & 0 & \lambda+2G \end{bmatrix}, \quad \tilde{\boldsymbol{C}}_{pn} = \tilde{\boldsymbol{C}}_{np}^{T} = \begin{bmatrix} 0 & 0 & \lambda \\ 0 & 0 & \lambda \\ 0 & 0 & 0 \end{bmatrix} \tag{17}$$

where G and λ are the Lamé's parameters. If Poisson's ratio ν and Young modulus E are used one has $G = \frac{E}{2(1+\nu)}$ and $\lambda = \frac{\nu E}{(1+\nu)(1-2\nu)}$.

Fundamental nuclei

The FE approach was adopted to discretize the structure along the y-axis. This process is conducted via a classical finite element technique, where the displacement vector is given by

$$\mathbf{u}(x,y,z) = F_\tau(x,z)N_i(y)\mathbf{q}_{\tau i} \tag{18}$$

N_i stands for the shape functions and $\mathbf{q}_{\tau i}$ for the nodal displacement vector,

$$\mathbf{q}_{\tau i} = \left\{ \begin{array}{ccc} q_{u_{x_{\tau i}}} & q_{u_{y_{\tau i}}} & q_{u_{z_{\tau i}}} \end{array} \right\}^T \tag{19}$$

For the sake of brevity, the shape functions are not reported here. They can be found in many books, for instance in (Bathe 1996). Elements with four nodes (B4) were adopted in this work, i.e. a cubic approximation along the y axis was assumed. The choice of the cross-section discretization for the LE class (i.e. the choice of the type, the number and the distribution of cross-section elements) or the theory order, N, for the TE class is completely independent of the choice of the beam finite element to be used along the axis of the beam.

The stiffness matrix of the elements and the external loadings vector were obtained via the principle of virtual displacements

$$\delta L_{int} = \int_V (\delta\boldsymbol{\epsilon}_p^T\boldsymbol{\sigma}_p + \delta\boldsymbol{\epsilon}_n^T\boldsymbol{\sigma}_n)dV = \delta L_{ext} \tag{20}$$

where L_{int} stands for the strain energy, L_{ext} is the work of the external loadings and δ stands for the virtual variation. The virtual variation of the strain energy was rewritten using Eq.s (13), (16) and (18):

$$\delta L_{int} = \delta \mathbf{q}_{\tau i}^T \mathbf{K}^{ij\tau s} \mathbf{q}_{sj} \tag{21}$$

where $\mathbf{K}^{ij\tau s}$ is the stiffness matrix in the form of the fundamental nucleus. In a compact notation, it can be written as:

$$\begin{aligned}
\boldsymbol{K}^{ij\tau s} \;=\; & I_l^{\;ij} \triangleleft \left(\boldsymbol{D}_{np}^T F_\tau \boldsymbol{I}\right)\Big[\tilde{\boldsymbol{C}}_{np}\left(\boldsymbol{D}_p F_s \boldsymbol{I}\right) \;+\; \tilde{\boldsymbol{C}}_{nn}\left(\boldsymbol{D}_{np} F_s \boldsymbol{I}\right)\Big] \;+ \\
& \left(\boldsymbol{D}_p^T F_\tau \boldsymbol{I}\right)\Big[\tilde{\boldsymbol{C}}_{pp}\left(\boldsymbol{D}_p F_s \boldsymbol{I}\right) \;+\; \tilde{\boldsymbol{C}}_{pn}\left(\boldsymbol{D}_{np} F_s \boldsymbol{I}\right)\Big] \triangleright_\Omega \;+ \\
& I_l^{ij,_y} \triangleleft \Big[\left(\boldsymbol{D}_{np}^T F_\tau \boldsymbol{I}\right)\tilde{\boldsymbol{C}}_{nn} \;+\; \left(\boldsymbol{D}_p^T F_\tau \boldsymbol{I}\right)\tilde{\boldsymbol{C}}_{pn}\Big] F_s \triangleright_\Omega \boldsymbol{I}_{\Omega y} \;+ \\
& I_l^{i,_y j} \boldsymbol{I}_{\Omega y} \triangleleft F_\tau \Big[\tilde{\boldsymbol{C}}_{np}\left(\boldsymbol{D}_p F_s \boldsymbol{I}\right) \;+\; \tilde{\boldsymbol{C}}_{nn}\left(\boldsymbol{D}_{np} F_s \boldsymbol{I}\right)\Big] \triangleright_\Omega \;+ \\
& I_l^{i,_y j,_y} \boldsymbol{I}_{\Omega y} \triangleleft F_\tau \tilde{\boldsymbol{C}}_{nn} F_s \triangleright_\Omega \boldsymbol{I}_{\Omega y}
\end{aligned} \tag{22}$$

where:

$$\boldsymbol{I}_{\Omega y} \;=\; \begin{bmatrix} 0 & 1 & 0 \\ 1 & 0 & 0 \\ 0 & 0 & 1 \end{bmatrix} \qquad\qquad \triangleleft \ldots \triangleright_\Omega \;=\; \int_\Omega \ldots \, d\Omega \tag{23}$$

$$\left(I_l^{\;ij},\, I_l^{ij,_y},\, I_l^{i,_y j},\, I_l^{i,_y j,_y}\right) \;=\; \int_l \left(N_i N_j,\; N_i N_{j,_y},\; N_{i,_y} N_j,\; N_{i,_y} N_{j,_y}\right) dy \tag{24}$$

The fundamental nucleus has to be expanded according to the summation indexes τ and s in order to obtain the elemental stiffness matrix. It should be noted that $\mathbf{K}^{ij\tau s}$ does not depend either on the expansion order or on the choice of the F_τ expansion polynomials. These are the key-points of CUF which allows, with only nine FORTRAN statements, the implementation of any-order of multiple class theories.

The loadings vector which is variationally coherent to the model was derived for the case

of a generic concentrated load $\mathbf{P}$ acting on the application point (x_p, y_p, z_p),

$$\mathbf{P} = \left\{ \begin{array}{ccc} P_{u_x} & P_{u_y} & P_{u_z} \end{array} \right\}^T \tag{25}$$

Any other loading condition can be similarly treated. The virtual work due to $\mathbf{P}$ is

$$\delta L_{ext} = \delta \mathbf{u}^T \mathbf{P} \tag{26}$$

After using Eq. (18), Eq. (26) becomes

$$\delta L_{ext} = F_\tau N_i \delta \mathbf{q}_{\tau i}^T \mathbf{P} \tag{27}$$

where F_τ and N_i are evaluated in (x_p, z_p) and y_p respectively. The last equation allows the identification of the components of the nucleus which have to be loaded, that is, it allows the proper assembling of the loading vector by detecting the displacement variables that have to be loaded.

NUMERICAL RESULTS

The effectiveness of the present CW formulation is evaluated in this section. Common I- and C-shaped beams are considered as initial assessments. The capability of the CW models to deal with very low aspect-ratio beams is then shown and used to model a transverse stiffening plate as a beam whose axis lays on the thickness direction. This characteristic of CW models, together with the possibility to impose localized constraints, is subsequently used to model a classical portal frame construction as a very short C-section beam. Next, more complex problems are addressed such as truss structures and a portal frame for industrial constructions. The results are compared to classical and higher-order TE beam theories and to FE models obtained via MSC Nastran.

I-section beam

The analysis of a cantilever I-shaped beam was carried out as the first assessment. The geometry of the cross-section is shown in Fig. 7. The dimensions of the beam are as follows: height $h = 100$ mm, width $w = 96$ mm, thickness of the flanges $t_1 = 8$ mm, thickness of the web $t_2 = 5$ mm. The length of the beam is $L = 1$ m. The structure is made of a steel alloy with Young's modulus, E, equal to 210 GPa and Poisson's ratio $\nu = 0.29$. A bending point load, $F_z = -2 \times 10^3$ N, was applied at $[\frac{w}{2}, L, \frac{h}{2}]$.

Table 1 shows the vertical displacement at the centroid of the tip cross-section and at the loaded point, together with the number of degrees of freedom (DOFs) for each model implemented. The Euler-Bernoulli theory is used, which leads to $u_{z_b} = \frac{F_z L^3}{3EI}$, where I is the cross-section moment of inertia. Classical and up to the eighth-order ($N = 8$) refined beam models based on Taylor-type expansion are also given in Table 1. The quoted CW model of the I-section beam was obtained by using 7 L9 elements on the cross-section as shown in Fig. 8, whereas 10 B4 elements were used along the beam axis. Beam, shell, and 3D solid MSC Nastran models are shown in the last two rows of Table 1. FEM Nastran models are used in this paper as benchmarks for comparison, and all of them were subjected to convergence analyses. An example is provided in Table 2, which shows the dependance of the solutions by the 1D beam, 2D shell and 3D solid NASTRAN models versus the mesh size for the problem under consideration. For each of the Nastran models, the number of elements, the number of DOFs, and the vertical displacement at the loaded point are given in the table. In Table 2, 2-node CBAR, 4-node CQUAD, and 8-node CHEXA elements were used for the beam, shell, and solid models, respectively.

Fig. 9 shows the deformed configuration of the tip cross-section for different structural models. It is clear from both Table 1 and Fig. 9 that classical beam models are not able to detect the mechanical behaviour of the structure for this problem. Torsional phenomenon and local effects are in fact not foreseen by these models and higher-order theories are therefore needed. Fig. 10 shows the cross-sectional distributions of axial and shear stress

components for both CW and Solid models. The figure shows that the CW model is able to correctly detect complex stress/strain fields in accordance with the 3D elasticity equations. Moreover, as a general remark, it should be underlined that the present formulation requires significantly lower computational efforts than a solid model.

C-shaped section with and without transverse stiffener and distributed and localized constraints

The C-shaped beam cross-section, which is shown in Fig. 11, has the following geometrical characteristics: sides $w = h = 0.2$ m, side-to-thickness of the flanges ratio $h/t = 10$. The whole structure is made of a steel alloy with Young's modulus (E) equal to 198 GPa and Poisson ratio $\nu = 0.3$.

Fig. 12 shows three different configurations whose results are discussed hereafter. In the first analysis case (Fig. 12a), the length of the beam is $L = 2$ m. The clamped-clamped (CC) beam undergoes a uniform pressure load equal to 1 MPa, which is applied at the top surface. Table 3 shows the vertical displacement at $x = 0$, $z = \frac{h}{2}$ on the mid-span cross-section and the normal stress component at the top right corner of the clamped end at $y = 0$. The number of DOFs are also given in the table for each model. Classical and higher-order TE theories as well as MSC Nastran models are shown for comparison purposes. The MSC Nastran models were obtained as in the previous example. Two different CW models of the CC C-shaped beam are provided in Table 3, differing from the number of L9 elements on the cross-section as shown in Fig. 13. In Fig. 13 a different notation with respect to Fig. 8 is adopted. In particular, the nodes of the L-elements are not depicted in Fig. 13 for the sake of simplicity. Fig. 14 shows the distribution of the vertical component of the displacement vector on the mid-span cross-section. CW models are compared to the fifth-order TE model and the 3D solution by MSC Nastran. The following comments arise from the analysis:

- Classical and lower-order TE models as well as Nastran Beam model are not able to correctly detect localized stress values.

- The 3D distributions of the displacement components can be affected by inaccuracies if thin-walled structures are analysed and higher-order TE theories are considered.
- As shown in (Carrera and Petrolo 2012a), CW models can be easily enhanced by enriching the displacement field, i.e. by increasing the number of L-elements on the cross-section.
- CW models are able to reproduce the 3D solutions with very low computational costs.

In recent works (Carrera et al. 2013d; Carrera et al. 2013a; Carrera et al. 2013b) the unique capability of the present 1D theories to deal with very low aspect ratio beams was demonstrated. In those papers 1D CUF models were in fact used to model reinforced thin-walled structures for aerospace applications. Here, a transverse stiffener is added to the C-shaped beam as shown in Fig. 12b. The effect of the "rib" is shown in Table 4, where both vertical and horizontal displacement components at different locations of the beam are given. In Table 4 the results by the CW approach are compared to a 2D and a 3D model by MSC Nastran. In the CW models, the transverse stiffener is modelled as a beam whose axis lays in the thickness direction. The CW cross-section discretizations of the rib are shown in Fig. 15. The rib is modelled with one B4 element along the beam axis. All the models given in the Table 4 show the undeformability of the cross-section close to the transverse stiffener. Conversely, the vertical flanges at $y = \frac{L}{4}$ are characterized by a non-null horizontal displacement as expected.

Another important characteristic of CW models is the possibility to deal with localized constraints, as shown in (Carrera and Petrolo 2012a). This feature, coupled with the capability to deal with very low aspect-ratio beams, allows for the modelling of the structure shown in Fig. 12c. In this analysis case, the portal undergoes a vertical point load $F_z = -40 \times 10^3$ N at $[0, \frac{t}{2}, \frac{h}{2}]$. Table 5 shows the vertical displacements at the loaded point and at $[0, 0, \frac{h}{2}]$, together with force reactions at the clamped ends and the number of DOFs. Force reactions are shown in Fig. 16 for the sake of clarity. Both CW and MSC Nastran models are given in Table 5. The Solid model was built by using 8-node CHEXA elements

as in the previous examples. The Nastran Beam model was obtained with 2-node CBAR elements, which are placed along three different beam-lines (two vertical and one horizontal axes). Conversely, the CW models were constructed by modelling the portal as a C-shaped cross-section beam with very low length $L = t = 0.02$ m. TE models are not given in Table 5 since the imposition of constraints at points which do not lay on the beam axis would involve the use of mathematical techniques such as the Lagrange multipliers method (see (Carrera et al. 2013c)). That being said, it is clear from the table that the present CW approach gives good results if compared to classical FE modelling approaches. Fig. 17 is finally given to definitely prove the capability of the present CW model in matching the solid solutions.

Truss structures

Truss structures are extensively used in bridge and industrial building constructions. Examples of the applicability of the present CW approach to the analysis of this class of structures are given hereinafter. The first example is shown in Fig. 18. A two-bay truss structure with a solid transverse stiffener is considered. The dimensions of the structure are: $h = w = 0.2$ m, $t = 0.02$ m, $L = 2$ m. The structure is made of the same steel alloy as in the previous example. A vertical point load, $F_z = -100$ N, is applied at the middle-span transverse stiffener at $x = 0$, $z = \frac{h}{2}$. Hinged supports were placed as shown in the figure.

Table 6 shows the vertical displacement at the loaded point and the axial stress component, σ_{yy}, at $[\frac{w}{2}, t, \frac{h}{2}]$. Both MSC Nastran and CW models are considered. Two different CW models are addressed. In the first case (Model A, Fig. 19a) the cross-section of the transverse stiffener was modelled with 9 L4 elements; each longitudinal *stringer* was modelled with one L4 element. In the second case (Model B, Fig. 19b) the transverse solid stiffener was modelled with 9 L9 elements and one L9 element was used for each stringer. The Nastran Beam/Shell model was obtained by using a combination of 1D 2-node CBAR and 2D 4-node CQUAD elements. In particular, beam elements were used to simulate the longitudinal frames and plate elements were used for the transverse stiffener. The results from a full solid Nastran model are also given in Table 6, together with the number of DOFs

for each model implemented.

Fig. 20 shows the same two-bay truss structure with hollow transverse stiffeners. Three different CW models are considered. In the CW Model A (Fig. 21a), the cross-section of the hollow transverse stiffener was modelled with a combination of L3, L4 and L9 elements. L4 elements were used for the stringers. In Model B (Fig. 21b), L3 and L9 elements were used on the cross-section of the stiffener, whereas L9 elements were used for the longitudinal frames. Finally, in Model C (Fig. 21c) the same discretization scheme of Model B was adopted but two L9 elements were used on the cross-section of the horizontal and vertical frames. The results by the CW models are shown in Table 7, together with FE solutions by MSC Nastran. The results from a Nastran solid model and a beam model are given for comparison purposes. Fig. 22 shows the 3D deformed configuration of the two-bay truss structure by the CW model. The analyses confirm what has been stated previously. In particular,

- The CW approach is effective in the analysis truss structures.
- The results by CW models agree with reference solutions by MSC Nastran both in terms of displacements and stresses.
- CW models provide solid-like results with very low computational costs.
- Both cross-sectional and longitudinal slender stiffening members as well as transverse stiffening plates can be modeled by the present CW approach. Panels cannot be modelled by classical truss type structural models.

Differences between classical FE beam models and the present 1D CW model should be underlined. In classical FE modeling, beam elements are placed along different beam-lines as shown in Fig. 23a. In CW approach, beam elements are placed along the longitudinal axis of the structure; for each beam node, the degrees of freedom are subsequently expanded above the cross-section components by using Lagrange polynomials (see Fig. 23b). In CW models, the unknowns are pure displacements and they can be placed on the physical surfaces of the

structure. This characteristic is a unique feature that makes this approach advantageous in a CAE/CAD scenario.

Typical portal frame construction for industrial buildings

A complete industrial building was considered as the last example. The structure is shown in Fig. 24. The main dimensions of the building are given in Table 8. Columns and frames have square section with side $t = 0.2$ m. The thickness of the roof is also equal to t. Two different load cases were addressed, as shown in Fig. 25. In the first load case (Fig. 25a), an horizontal load, $F_x = -2 \times 10^3$ N, was applied. In the second load case (Fig. 25b), the structure also underwent a gravity load, which is considered as a uniform vertical pressure distribution ($q_z = 960$ Pa).

For both load cases, table 9 shows the displacement and stress components and the number of DOFs for each model. CW models are compared to a full MSC Nastran solid model and a FE model obtained by using a combination of 1D beam and 2D plate elements. In particular, the Beam/Shell Nastran model was obtained by using 2-node CBAR beam elements to model columns and frame and CQUAD elements for the roof. The CW model was constructed by considering the whole structure as a beam laying along the y-axis (see Fig. 24). Two different cross-sectional combinations of L-elements were used in the CW beam modelling and they are shown in Fig. 26. The sole difference between Model A (Fig. 26a) and Model B (Fig. 26b) is that 4 L9 instead of 2 L9 elements are used in Model B to discretize the columns. The capability to enrich the displacement field of the single component is one of the main feature of the present CW model and it is clear from the proposed analyses. Fig. 27 finally shows the deformation of the loaded cross-section from both CW and Solid models for Load Case 1. The computational efficiency of the proposed CW models with respect to the MSC Nastran solid model is evident. Moreover, it should definitely noted the unique capability of the present CW approach, which allows to model each of the structure's components (i.e. columns, frame members, and roof) with the same 1D element, without the need of adopting different kinematics. As a consequence, artificial lines (beam axes) and

surfaces (plate/shell reference surfaces) are no longer used. This is otherwise possible only if 3D solid elements are adopted.

CONCLUSIONS

In this paper, the CW approach has been presented and used to carry out analyses of typical civil engineering structures. The main novelty introduced by the present CW models is that each structural component such as frame members, columns, transverse stiffening plates, flanges and webs can be modeled with the same 1D finite element. Moreover, it has been shown that CW models preserve their efficacy when applied to complex truss structures and portal frame industrial buildings. The results have been successfully compared to classical and refined beam theories indeed as well as to FE models built by means of the commercial software MSC Nastran. Three-dimensional FE analysis is required to reach the same accuracy of CW with a number of DOFs which is at least one order of magnitude higher than the present models.

Future work should deal with the extension of the proposed approach to include physical and geometrical non-linearities as well as ultimate load analysis.

REFERENCES

Bathe, K. J. (1996). *Finite element procedure*. Prentice hall.

Bebiano, R., Silvestre, N., and Camotim, D. (2008). "Local and global vibration of thin-walled members subjected to compression and non-uniform bending." *Journal of Sound and Vibration*, 345, 509–535.

Berdichevsky, V. L., Armanios, E., and Badir, A. (1992). "Theory of anisotropic thin-walled closed-cross-section beams." *Composites Engineering*, 2(5–7), 411–432.

Carrera, E., Giunta, G., Nali, P., and Petrolo, M. (2010). "Refined beam elements with arbitrary cross-section geometries." *Computers and Structures*, 88(5–6), 283–293 DOI: 10.1016/j.compstruc.2009.11.002.

Carrera, E., Giunta, G., and Petrolo, M. (2011a). *Beam Structures: Classical and Advanced Theories*. John Wiley & Sons DOI: 10.1002/9781119978565.

Carrera, E., Maiarú, M., and Petrolo, M. (2012a). "Component-wise analysis of laminated anisotropic composites." *International Journal of Solids and Structures*, 49, 1839–1851 DOI: 10.1016/j.ijsolstr.2012.03.025.

Carrera, E., Pagani, A., and Petrolo, M. (2013a). "Classical, refined and component-wise theories for static analysis of reinforced-shell wing structures." *AIAA Journal*, 51(5), 1255–1268 DOI: 10.2514/1.J052331.

Carrera, E., Pagani, A., and Petrolo, M. (2013b). "Component-wise method applied to vibration of wing structures." *Journal of Applied Mechanics*, 80(4), 041012–1 – 041012–15 DOI: 10.1115/1.4007849.

Carrera, E., Pagani, A., and Petrolo, M. (2013c). "Use of Lagrange multipliers to combine 1D variable kinematic finite elements." *Computers and Structures* DOI: 10.1016/j.compstruc.2013.07.005. In Press.

Carrera, E., Pagani, A., Petrolo, M., and Zappino, E. (2012b). "A component-wise approach in structural analysis." *Computational Methods for Engineering Science*, B. H. V. Topping, ed., Saxe-Coburg Publications, Chapter 4, 75–115. DOI: 10.4203/csets.30.4.

Carrera, E. and Petrolo, M. (2012a). "Refined beam elements with only displacement variables and plate/shell capabilities." *Meccanica*, 47(3), 537–556 DOI: 10.1007/s11012-011-9466-5.

Carrera, E. and Petrolo, M. (2012b). "Refined one-dimensional formulations for laminated structure analysis." *AIAA Journal*, 50(1), 176–189 DOI: 10.2514/1.J051219.

Carrera, E., Petrolo, M., and Nali, P. (2011b). "Unified formulation applied to free vibrations finite element analysis of beams with arbitrary section." *Shock and Vibrations*, 18(3), 485–502 DOI: 10.3233/SAV-2010-0528.

Carrera, E., Petrolo, M., and Varello, A. (2012c). "Advanced beam formulations for free vibration analysis of conventional and joined wings." *Journal of Aerospace Engineering*, 25(2), 282–293 DOI: 10.1061/(ASCE)AS.1943-5525.0000130.

Carrera, E., Petrolo, M., and Zappino, E. (2012d). "Performance of CUF approach to analyze

the structural behavior of slender bodies." *Journal of Structural Engineering*, 138(2), 285–297 DOI: 10.1061/(ASCE)ST.1943-541X.0000402.

Carrera, E., Zappino, E., and Petrolo, M. (2013d). "Analysis of thin-walled structures with longitudinal and transversal stiffeners." *Journal of Applied Mechanics*, 80, 011006–1–011006–12 DOI: 10.1115/1.4006939.

El Fatmi, R. (2002). "On the structural behavior and the Saint Venant solution in the exact beam theory: application to laminated composite beams." *Computers and Structures*, 80(16–17), 1441–1456.

El Fatmi, R. (2007a). "Non-uniform warping including the effects of torsion and shear forces. Part I: a general beam theory." *International Journal of Solids and Structures*, 44(18–19), 5912–5929.

El Fatmi, R. (2007b). "Non-uniform warping including the effects of torsion and shear forces. Part II: analytical and numerical applications." *International Journal of Solids and Structures*, 44(18–19), 5930–5952.

Euler, L. (1744). *De curvis elasticis*. Lausanne and Geneva: Bousquet (English translation: W. A. Oldfather, C. A. Elvis, D. M. Brown, Leonhard Euler's elastic curves, Isis 20 (1933) 72–160).

Firouz-Abad, R. D., Haddadpour, H., and Novinzadehb, A. B. (2007). "An asymptotic solution to transverse free vibrations of variable-section beams." *Journal of Sound and Vibration*, 304, 530–540.

Kapania, K. and Raciti, S. (1989a). "Recent advances in analysis of laminated beams and plates, part I: Shear effects and buckling." *AIAA Journal*, 27(7), 923–935.

Kapania, K. and Raciti, S. (1989b). "Recent advances in analysis of laminated beams and plates, part II: Vibrations and wave propagation." *AIAA Journal*, 27(7), 935–946.

Kim, C. and White, S. R. (1997). "Thick-walled composite beam theory including 3-D elastic effects and torsional warping." *International Journal of Solids and Structures*, 34(31–32), 4237–4259.

Kim, J. S. and Wang, K. W. (2010). "Vibration analysis of composite beams with end effects via the formal asymptotic method." *Journal of Vibration and Acoustics*, 132(4), 041003.

Ladéveze, P., Sanchez, P., and Simmonds, J. (2004). "Beamlike (Saint-Venant) solutions for fully anisotropic elastic tubes of arbitrary closed cross-section." *International Journal of Solids and Structures*, 41(7), 1925–1944.

Ladéveze, P. and Simmonds, J. (1998). "New concepts for linear beam theory with arbitrary geometry and loading." *European Journal Of Mechanics A/Solids*, 17(3), 377–402.

Novozhilov, V. V. (1961). *Theory of elasticity*. Pergamon, Elmsford.

Oñate, E. (2009). *Structural Analysis with the Finite Element Method: Linear Statics, Volume 1*. Springer.

Petrolo, M., Zappino, E., and Carrera, E. (2012). "Refined free vibration analysis of one-dimensional structures with compact and bridge-like cross-sections." *Thin-Walled Structures*, 56, 49–61 DOI: 10.1016/j.tws.2012.03.011.

Popescu, B. and Hodges, D. H. (2000). "On asymptotically correct Timoshenko-like anisotropic beam theory." *International Journal of Solids and Structures*, 37, 535–558.

Rand, O. (1994). "Free vibration of thin-walled composite blades." *Composite Structures*, 28, 169–180.

Schardt, R. (1966). "Eine erweiterung der technischen biegetheorie zur berechnung prismatischer faltwerke (Extension of the engineer's theory of bending to the analysis of folded plate structures)." *Der Stahlbau*, 35, 161–171.

Schardt, R. (1994). "Generalized beam theory an adequate method for coupled stability problems." *Thin-Walled Structures*, 19, 161–180.

Silvestre, N. (2002). "Second-order generalised beam theory for arbitrary orthotropic materials." *Thin-Walled Structures*, 40(9), 791–820.

Silvestre, N. (2007). "Generalised beam theory to analyse the buckling behaviour of circular cylindrical shells and tubes." *Thin-Walled Structures*, 45(2), 185–198.

Silvestre, N. and Camotim, D. (2002). "First-order generalised beam theory for arbitrary

orthotropic materials." *Thin-Walled Structures*, 40(9), 755–789.

Timoshenko, S. P. (1922a). "On the corrections for shear of the differential equation for transverse vibrations of prismatic bars." *Philosophical Magazine*, 41, 744–746.

Timoshenko, S. P. (1922b). "On the transverse vibrations of bars of uniform cross section." *Philosophical Magazine*, 43, 125–131.

Vlasov, V. Z. (1961). *Thin-walled elastic beams*. National Science Foundation, Washington.

Volovoi, V. V., Hodges, D. H., Berdichevsky, V. L., and Sutyrin, V. G. (1999). "Asymptotic theory for static behavior of elastic anisotropic I-beams." *International Journal of Solids and Structures*, 36, 1017–1043.

Washizu, K. (1968). *Variational Methods in Elasticity and Plasticity*. Pergamon, Oxford.

Yu, W. and Hodges, D. H. (2004). "Elasticity solutions versus asymptotic sectional analysis of homogeneous, isotropic, prismatic beams." *Journal of Applied Mechanics*, 71, 15–23.

Yu, W. and Hodges, D. H. (2005). "Generalized Timoshenko theory of the variational asymptotic beam sectional analysis." *Journal of the American Helicopter Society*, 50(1), 46–55.

Yu, W., Volovoi, V. V., Hodges, D. H., and Hong, X. (2002). "Validation of the variational asymptotic beam sectional analysis (VABS)." *AIAA Journal*, 40, 2105–2113.

TABLES

FIGURES

	$-u_z(0, L, 0)$, mm	$-u_z(\frac{w}{2}, L, \frac{h}{2})$, mm	DOFs
$-u_{z_b} = \frac{F_z L^3}{3EI} = 0.951$, mm			
Classical and refined beam theories based on TE			
EBBM	0.951	0.951	93
TBM	0.964	0.964	155
$N = 1$	0.964	0.978	279
$N = 2$	0.956	0.978	558
$N = 3$	0.989	1.018	930
$N = 4$	0.989	1.287	1395
$N = 5$	0.993	1.481	1953
$N = 6$	0.992	1.462	2604
$N = 7$	0.997	1.560	3348
$N = 8$	0.997	1.851	4185
Present CW model			
7 L9, Fig. 8	0.953	2.213	4185
MSC Nastran models			
Beam	0.961	0.961	60
Shell	0.959	2.321	61000
Solid	0.956	2.316	355800

TABLE 1. Vertical displacement at the centroid of the tip cross-section, $u_z(0, L, 0)$, and at the loaded point, $u_z(\frac{w}{2}, L, \frac{h}{2})$, for the I-section beam (Fig. 7)

Beam			Shell			Solid		
No. Elmts.	DOFs	$-u_z^*$	No. Elmts.	DOFs	$-u_z^*$	No. Elmts.	DOFs	$-u_z^*$
10	60	0.961	900	4750	2.308	1800	11100	2.260
50	300	0.961	3000	15500	2.312	11300	55200	2.286
100	600	0.961	12000	61000	2.321	90400	355800	2.316

*: $-u_z(\frac{w}{2}, L, \frac{h}{2})$, mm

TABLE 2. Mesh dependance of reference MSC Nastran solutions, I-section beam (Fig. 7)

	$-u_z$, mm	$\sigma_{yy} \times 10^{-2}$, MPa	DOFs
Classical and refined beam theories based on TE			
EBBM	0.925	1.088	93
TBM	1.041	1.088	155
$N = 1$	1.041	1.088	279
$N = 2$	1.022	1.306	558
$N = 3$	1.073	2.009	930
$N = 4$	1.091	1.892	1395
$N = 5$	1.102	1.864	1953
Present CW models			
8 L9, Fig. 13a	1.112	1.949	4185
14 L9, Fig. 13b	1.138	1.963	8091
MSC Nastran models			
Beam	1.141	1.094	594
Shell	1.115	2.083	60695
Solid	1.208	2.217	337305

TABLE 3. Vertical displacement, u_z, at $[0, \frac{L}{2}, \frac{h}{2}]$ and normal stress component, σ_{yy}, at $[\frac{w}{2}, 0, \frac{h}{2}]$ for the CC C-section beam (Fig. 12a)

	$-u_z$, mm	u_x, mm		DOFs
		$[\frac{w}{2}, \frac{L}{2}, 0]$	$[\frac{w}{2}, \frac{L}{4}, 0]$	
Present CW models				
Model A, Fig. 15a	1.165	0.000	0.047	5346
Model B, Fig. 15b	1.169	0.000	0.072	9546
MSC Nastran models				
Shell	1.028	0.000	0.110	62595
Solid	1.121	0.000	0.112	294525

TABLE 4. Effect of the transverse stiffener on the CC C-section beam (Fig. 12b). Vertical displacement, u_z, at $[0, \frac{L}{2}, \frac{h}{2}]$ and horizontal displacement, u_x, at $[\frac{w}{2}, \frac{L}{2}, 0]$ and $[\frac{w}{2}, \frac{L}{4}, 0]$

	$-u_z(0,0,h/2)$, mm	$-u_z(0,t/2,h/2)$, mm	$R_x \times 10^{-4}$, N	$R_z \times 10^{-4}$, N	DOFs
		Present CW models			
8 L9	0.729	0.742	0.545	2.000	1071
14 L9	0.926	0.951	0.507	2.000	1827
		MSC Nastran models			
Beam	1.065	1.065	0.456	2.000	354
Solid	0.975	1.034	0.489	2.000	8325

TABLE 5. Vertical displacements, u_z, at $[0, 0, \frac{h}{2}]$ and at $[0, \frac{L}{2}, \frac{h}{2}]$ and reactions at the clamped ends (see Fig. 16) for the very short C-section beam (Fig. 12c)

	$-u_z$, mm	σ_{yy}, MPa	DOFs
Present CW models			
Model A, Fig. 19a	0.839	3.738	1632
Model B, Fig. 19b	0.984	4.119	4140
MSC Nastran models			
Beam/Shell	1.128	4.124	19163
Solid	1.019	3.187	127785

TABLE 6. Vertical displacement at $[0, \frac{L}{2}, \frac{h}{2}]$ and normal stress at $[\frac{w}{2}, t, \frac{h}{2}]$ for the two-bay truss structure with solid transverse stiffener (Fig. 18)

	$-u_z$, mm	DOFs
Present CW models		
Model A, Fig. 21a	0.880	3828
Model B, Fig. 21b	1.015	6732
Model C, Fig. 21c	1.026	7596
MSC Nastran models		
Beam	1.065	7562
Solid	1.050	98760

TABLE 7. Vertical displacement at $[0, \frac{L}{2}, \frac{h}{2}]$ for the two-bay truss structure with hollow transverse stiffener (Fig. 20)

	Dimensions, m
Length, L	14.00
Width, w	13.80
h_1	7.00
h_2	3.00
c	4.50

TABLE 8. Main dimensions of the portal frame industrial construction (Fig. 24)

	Load Case 1	Load Case 2			
	$-u_x^a$, mm	$-u_x$, mm	$-u_z^b$, mm	$-\sigma_{zz}^c$, MPa	DOFs
Present CW models					
Model A, Fig. 26a	0.713	0.709	0.716	1.591	6543
Model B, Fig. 26b	0.893	0.869	0.730	1.541	7119
MSC Nastran models					
Beam/Shell	0.865	0.812	0.723	1.546	2835
Solid	0.858	0.799	0.719	1.558	143121

[a]: u_x measured at F_x load application point

[b]: u_z measured at $[w, \frac{L}{2}, h]$

[c]: maximum σ_{zz} component value in the column at $x = w$, $y = 0$

TABLE 9. Displacement and stress components for different load cases, portal frame industrial construction (Fig 24)

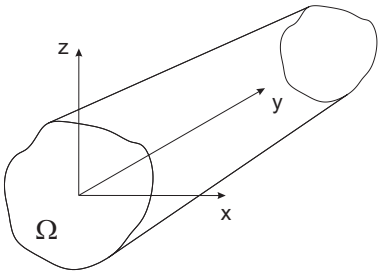

FIG. 1. Coordinate frame of the beam model

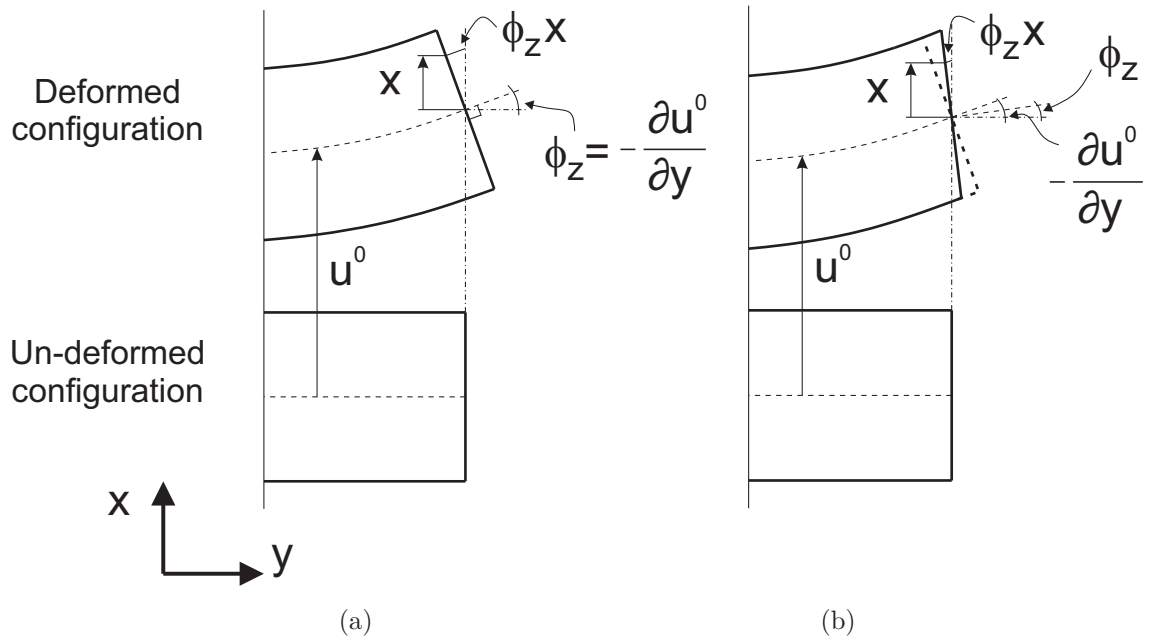

FIG. 2. Differences between Euler-Bernoulli (a) and Timoshenko (b) beam theories

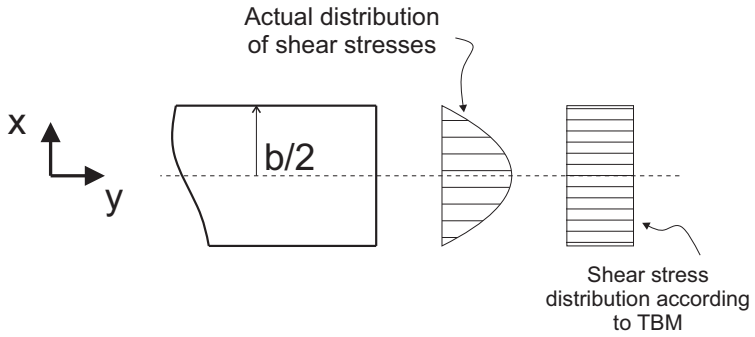

FIG. 3. Limit condition of transverse stress components

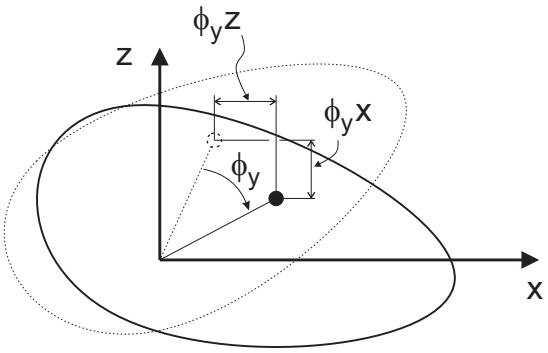

FIG. 4. Rigid torsion of the beam cross-section

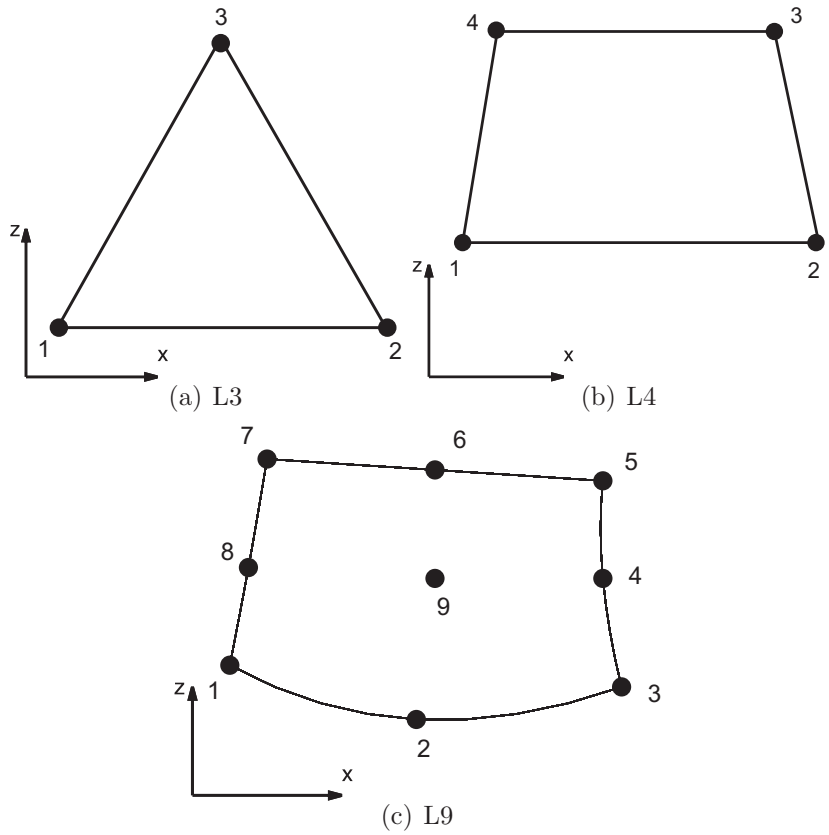

(a) L3 (b) L4

(c) L9

FIG. 5. Cross-sectional Lagrange polynomial sets

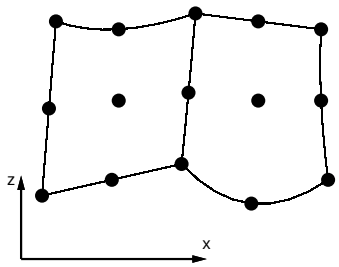

FIG. 6. Two assembled L9 elements in actual geometry

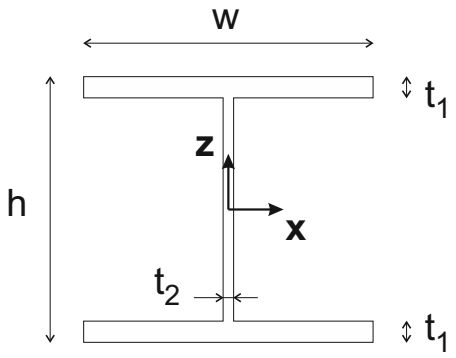

FIG. 7. Cross-section of the I-section beam

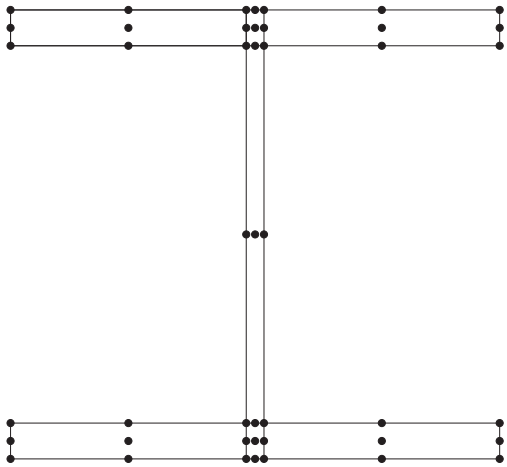

FIG. 8. Distribution of the 7 L9 elements above the cross-section of the I-shaped beam

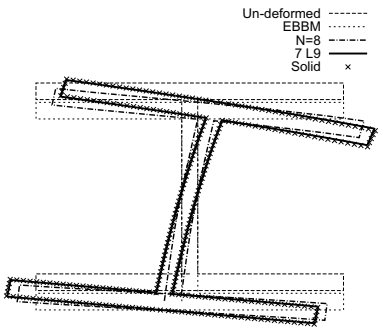

FIG. 9. Deformed tip cross-section of the I-section beam

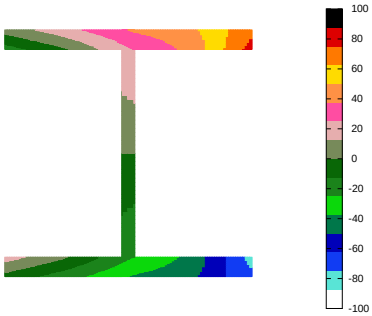

(a) σ_{yy} at $y = 0$, CW 7 L9 model

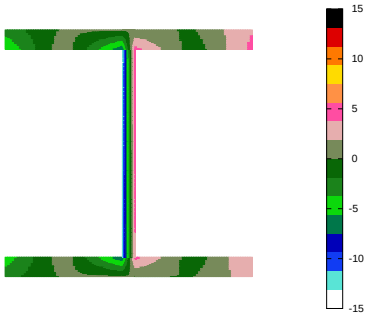

(b) σ_{yz} at $y = \frac{L}{2}$, CW 7 L9 model

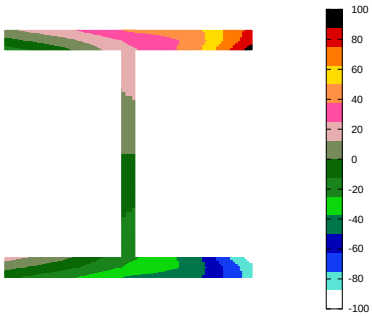

(c) σ_{yy} at $y = 0$, Solid model

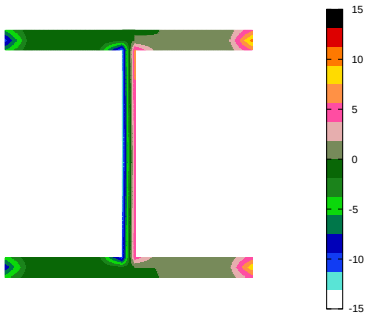

(d) σ_{yz} at $y = \frac{L}{2}$, Solid model

FIG. 10. Distribution of axial, σ_{yy}, and transversal, σ_{yz}, stresses for the I-section beam. Comparison between CW and Solid models

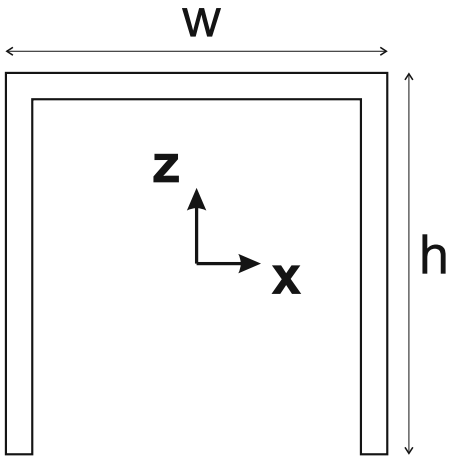

FIG. 11. Cross-section of the C-shaped beam

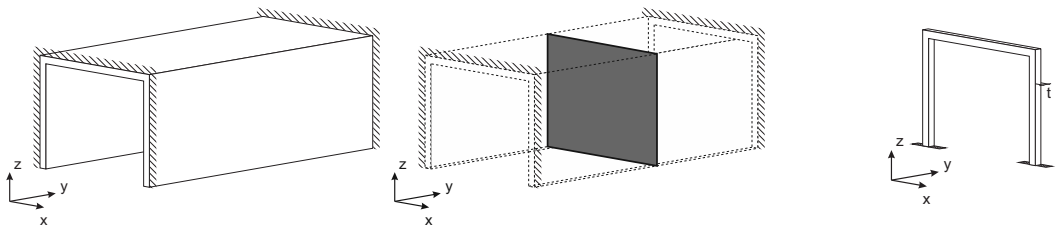

(a) CC C-shaped beam (b) C-shaped beam with transverse stiffener (c) very short C-shaped beam with localized constraints

FIG. 12. Various configurations of the C-shaped beam

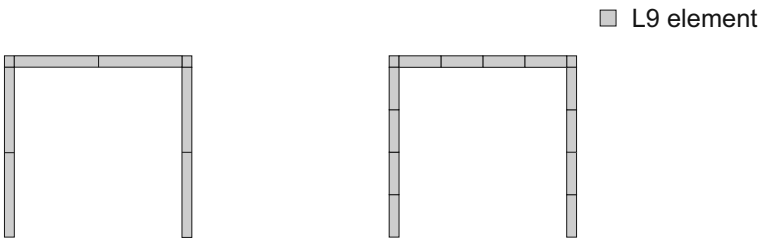

(a) 8 L9 (b) 14 L9

FIG. 13. Distribution of L-elements on the cross-section of the C-shaped beam

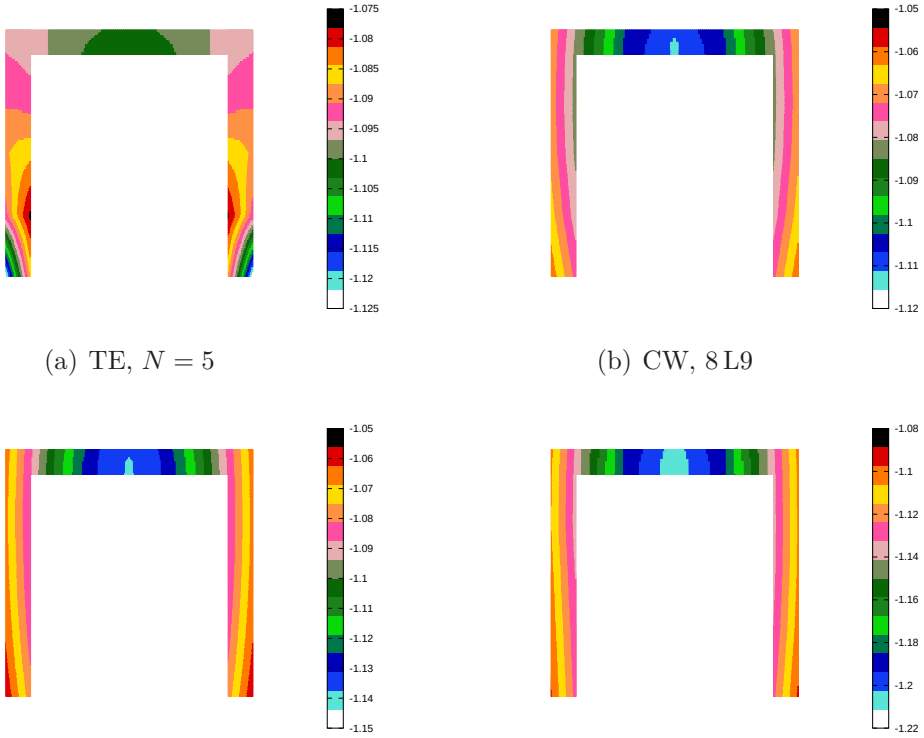

(a) TE, $N = 5$

(b) CW, 8 L9

(c) CW, 14 $L9$

(d) Solid model

FIG. 14. Distribution of the vertical displacement, u_z, on the mid-span cross-section for the C-shaped beam (Fig. 12a)

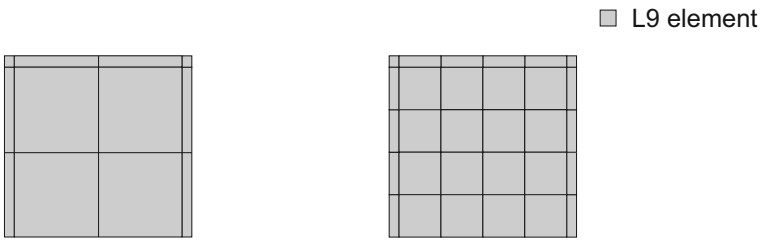

(a) Model A (b) Model B

FIG. 15. L-elements distribution on the cross-section of the transverse stiffener, CC C-shaped beam (Fig. 12b)

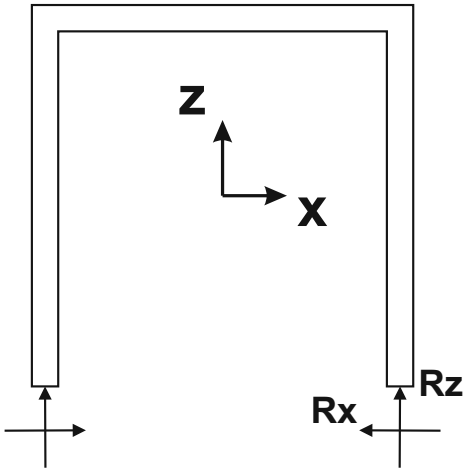

FIG. 16. Force reactions of the very short C-shaped beam (Fig. 12c)

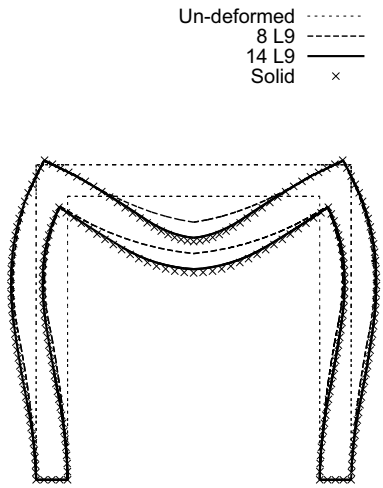

FIG. 17. Deformed cross-section at $y = 0$. Very short C-shaped beam (Fig. 12c)

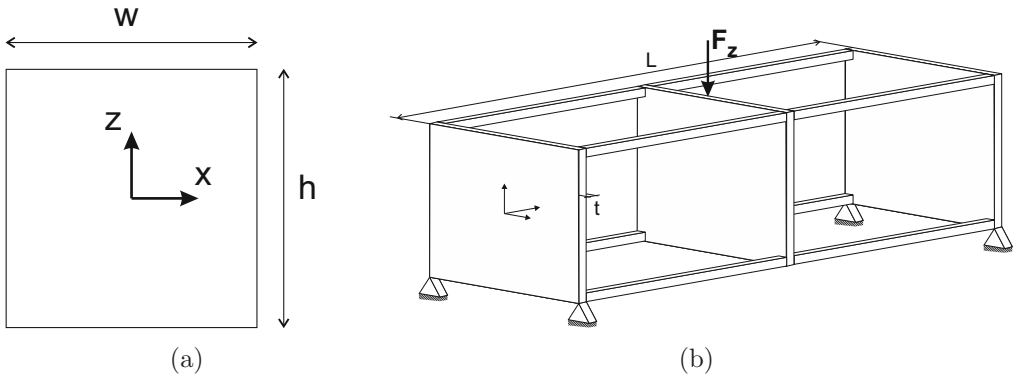

(a) (b)

FIG. 18. Cross-section geometry and loading condition of the two-bay truss structure with solid transverse stiffener

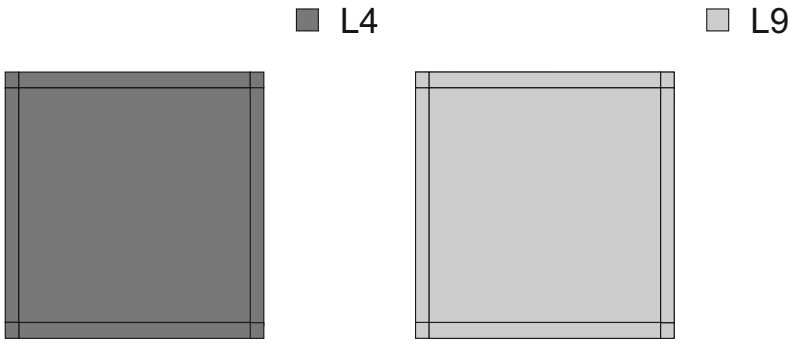

(a) Model A (b) Model B

FIG. 19. Cross-sectional distributions of L-elements on the solid transverse stiffener of the truss structure

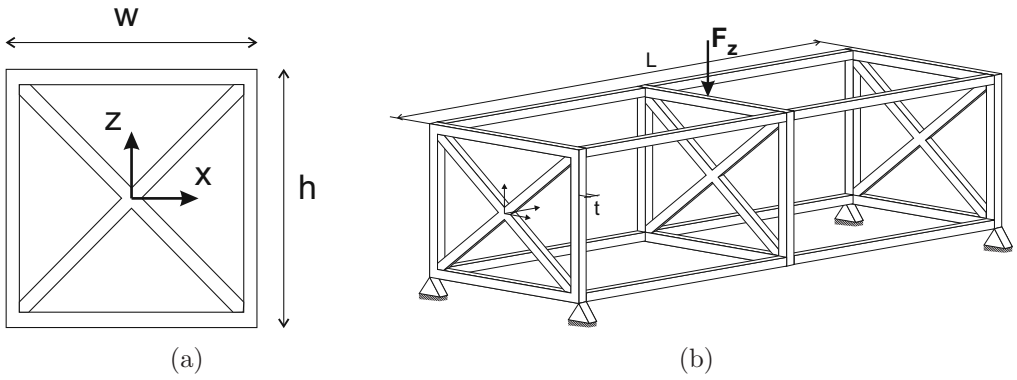

FIG. 20. Two-bay truss structure with hollow transverse stiffener

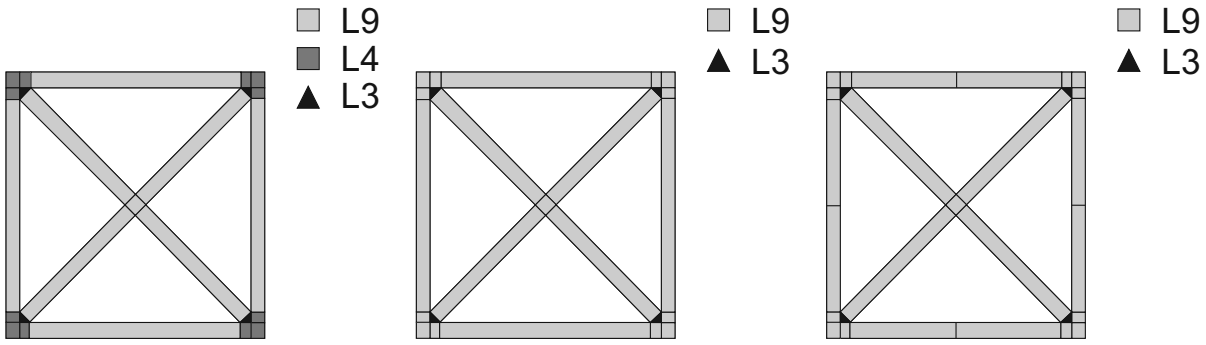

(a) Model A (b) Model B (c) Model C

FIG. 21. Cross-sectional distribution of L-elements for the CW models of the two-bay truss structure with hollow transverse stiffener

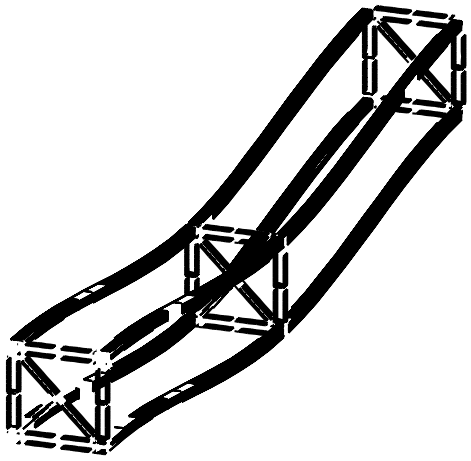

FIG. 22. 3D deformation of the two-bay truss structure by CW, Model C (Fig. 21c)

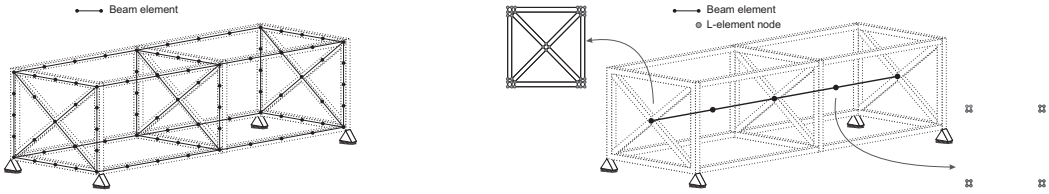

(a) Classical FEs (b) CW approach

FIG. 23. Differences between classical FE beam modelling and CW approach

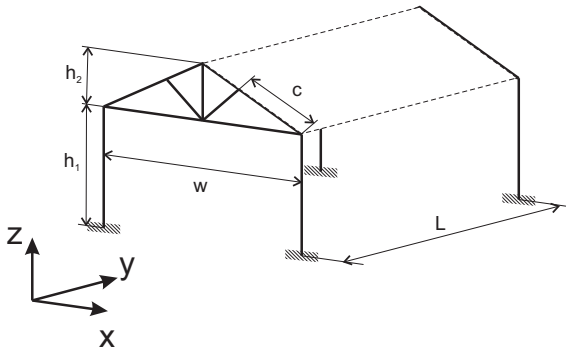

FIG. 24. Geometry of the portal frame construction

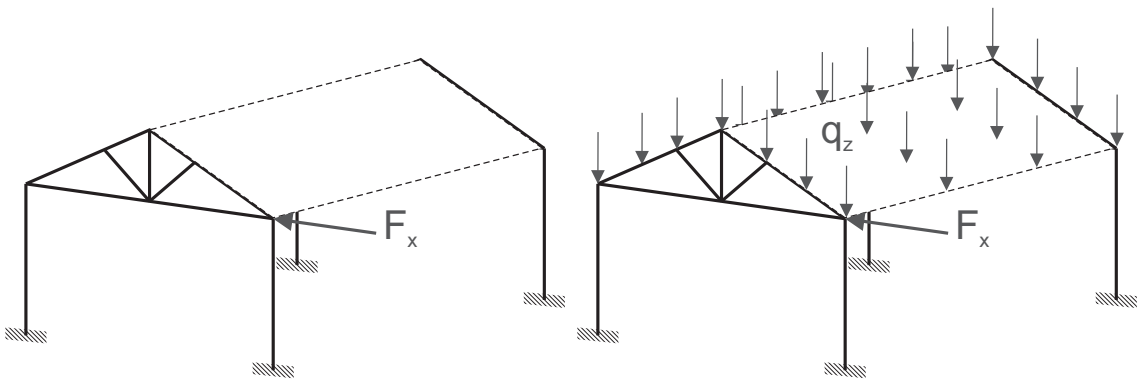

(a) Load Case 1 (b) Load Case 2

FIG. 25. Loading configurations applied to the portal frame construction

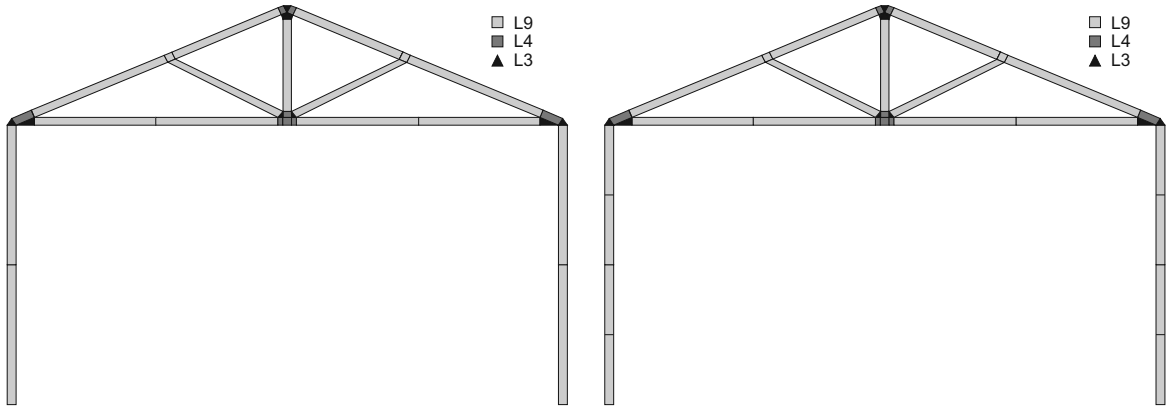

(a) Model A (b) Model B

FIG. 26. L-elements distribution on the cross-section for the CW model of the portal frame industrial construction

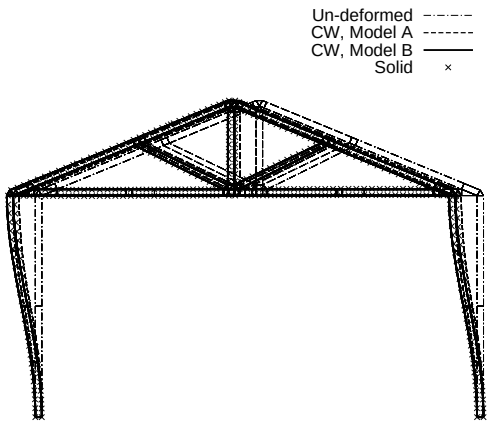

FIG. 27. Deformation of the loaded cross-section of the portal frame industrial construction (Fig. 25)